Algebraic dynamic multilevel method for fractured geothermal reservoir simulation

HosseiniMehr, Mousa; Arbarim, Rhadityo; Cusini, Matteo; Vuik, Cornelis; Hajibeygi, Hadi

DOI
10.2118/193894-MS

Publication date
2019

Document Version
Final published version

Published in
Society of Petroleum Engineers - SPE Reservoir Simulation Conference 2019, RSC 2019

SPE-193894-MS

Algebraic Dynamic Multilevel Method for Fractured Geothermal Reservoir Simulation

Mousa HosseiniMehr, Rhadityo Arbarim, Matteo Cusini, Cornelis Vuik, and Hadi Hajibeygi, Delft University of Technology

This paper was prepared for presentation at the SPE Reservoir Simulation Conference held in Galveston, Texas, USA, 10–11 April 2019.

Abstract

A dynamic multilevel method for fully-coupled simulation of flow and heat transfer in heterogeneous and fractured geothermal reservoirs is presented (FG-ADM). The FG-ADM develops an advanced simulation method which maintains its efficiency when scaled up to field-scale applications, at the same time, it remains accurate in presence of complex fluid physics and heterogeneous rock properties. The embedded discrete fracture model is employed to accurately represent fractures without the necessity of unstructured complex grids. On the fine-scale system, FG-ADM introduces a multi-resolution nested dynamic grid, based on the dynamic time-dependent solution of the heat and mass transport equations. The fully-coupled implicit simulation strategy, in addition to the multilevel multiscale framework, makes FG-ADM to be stable and efficient in presence of strong flow-heat coupling terms. Furthermore, its finite-volume formulation preserves local conservation for both mass and heat fluxes. Multi-level local basis functions for pressure and temperature are introduced, in order to accurately represent the heterogeneous fractured rocks. These basis functions are constructed at the beginning of the simulation, and are reused during the entire dynamic time-dependent simulation. For several heterogeneous test cases with complex fracture networks we show that, by employing only a fraction of the fine-scale grid cells, FG-ADM can accurately represent the complex flow-heat solutions in the fractured subsurface formations.

Introduction

Geothermal energy resources are attractive due to their low carbon footprints (Bertani, 2012; Lund et al., 2011; Burnell et al., 2012, 2015). Having the potential of providing more sustainable energy, compared with hydrocarbons, the demands for geothermal energy is expected to increase over the next couple of decades. Development of accurate scalable simulation methods for fluid flow in geothermal reservoirs is important to fulfill the societal (including productivity estimation) expectations for successful operational managements (Moraes et al., 2017; McClure and Horne, 2014).

Field-applicable simulation tools should accurately capture high contrasts in the fluid and heat transport properties within the reservoir, specially in presence of fractures and faults. This imposes severe computational challenges, because it demands for imposing high-resolution computational grids over the

entire large-scale (km) computational geo-models (Praditia et al., 2018). In addition, nonlinear strongly coupled flow-heat processes lead to stability and convergence issues, specially in presence of phase change (steam-water flow) (Wong et al., 2018). Moreover, the presence of fractures add to the complexity due to their severe property contrasts compared to their hosting geological rocks. Geo-chemical interactions between solid rock and fluid (Morel and Morgan, 1972; Leal et al., 2017) together with geo-mechanical effects (Rossi et al., 2018; Garipov et al., 2016) are also among the important challenges. These challenges motivate the development of advanced simulation methods that maintain their accuracy and efficiency (stability and scalability) when applied to large-scale field-relevant applications (Fung and Dogru, 2007; Dogru et al., 2009).

In this article, a scalable and efficient simulation method for fluid flow in fractured geothermal reservoirs is introduced. To ensure stability in presence of strong nonlinear physics, a Fully-IMplicit (FIM) coupling approach is followed (Younis et al., 2010). Entries of the fine-scale FIM system include three sets of equations for conservation of mass, fluid energy and rock energy balance. Explicit fractures are modelled by the Embedded Discrete Fracture Model (Lee et al., 1999, 2001; Li and Lee, 2008; Hajibeygi et al., 2011a; Moinfar et al., 2014; Fumagalli et al., 2016, 2017). Note that the recently introduced projection EDFM (pEDFM) method formulates a consistent embedded discrete approach (Tene et al., 2017) for all fracture-matrix conductivity contrasts. The choice of EDFM is motivated by its convenient formulation and flexible grid geometries (Norbeck et al., 2016; Shah et al., 2016). It allows, e.g., to generate independent grids for matrix and fractures, though (as in other computational methods) grid resolution should be adjusted to maintain the expected numerical accuracy (Pluimers, 2015; Jiang and Younis, 2016).

This EDFM-based FIM discrete system is obtained for pressure, fluid temperature and solid rock temperature as the main unknowns. Note that for most (or perhaps all) of the geoscience applications, one can safely assume local thermal equilibrium, under which the fluid and rock temperatures would be equal. Here, to keep the general framework intact, local thermal non-equilibrium is also allowed (Coats, 1977).

The fine-scale system considers both conductive and convective heat transfer terms, and, as described, allows for different temperature values for fluid and solid rock. In linear simulation stage, it is convenient to sum the two energy balance equations to obtain one (average) temperature value for both fluid temperature and solid rock temperature. This allows for reduction of the main unknowns, and is done for the simulation results of this work.

Even with EDFM-based strategy, the classical FIM systems become too expensive to be solved in real-field applications. Upscaling the nonlinear formulations does not lead to good approximate solutions and similarly sensitive systems with the user-defined error control strategies (Cusini et al., 2018b). In this work, a fully-implicit multilevel multiscale approach is presented to solve this challenge.

On the obtained EDFM-FIM system for fractured heterogeneous geothermal geo-models, at each time step, a hierarchical multilevel resolution is imposed. The hierarchical resolutions are obtained based on the zone of interest, typically imposed by the fronts within the solution of the local unknowns. This is the same strategy as in the Adaptive Mesh Refinement (AMR) methods (Bell and Shubin, 1983; Berger and Oliger, 1984; Hornung and Trangenstein, 1997; Edwards, 1996; Schmidt and Jacobs, 1988; Sammon, 2003; van Batenburg et al., 2011; Faigle et al., 2014). The offline (preprocessing step) locally computed multiscale basis functions are used to map the global solution between the hierarchical grids. The locally computed basis functions maintain the accuracy of the solutions even for highly heterogeneous reservoirs. The basis functions and construction of the multilevel dynamic FIM system are employed algebraically (Cusini et al., 2016). As such, the method inherits the term algebraic in its definition. This Algebraic Dynamic Multilevel (ADM) method is capable of capturing physics of flow and heat transfer at fine-scale resolution close to the sharp gradients, while for the rest of the domain, basis functions will provide accurate approximate solutions. A user-defined threshold for the accuracy of the method is allowed, meaning that the procedure is self-adaptive in selection of the hierarchical nested grids in order to maintain the required accuracy.

The local basis functions are constructed on multiple coarsening levels for all unknown (i.e., pressure, fluid temperature and solid rock temperature) at the beginning of the simulation. Here, structured grids are used at all levels, and the original multiscale basis functions (Hou and Wu, 1997; Jenny et al., 2003; Hajibeygi et al., 2008) with their algebraic descriptions (Wang et al., 2014) are employed for pressure and solid rock temperature (conductive heat transfer), while constant interpolation functions (conductive-convective) are used for fluid temperature on all coarsening levels. One can also use multiscale-based bases for fluid heat transfer (Praditia et al., 2018) with adaptive local supports (Klemetsdal et al., 2018). We reiterate that, in this work, all local basis functions are calculated only at the very beginning of the simulation (offline pre-processing stage) and will not be updated throughout the entire simulation time at all. It is worth to be mentioned that a homogenisation-based basis function for ADM has been introduced recently (Singh et al., 2018).

Numerical results for both homogeneous and heterogeneous test-cases are presented to demonstrate the accuracy and applicability of this method.

The paper is organised as following. The governing equations together with the fine-scale discrete systems are presented in Section 1. The ADM methodology for fractured geothermal simulation is then presented in Section 2. Numerical results are reported in Section 3. The paper is finally concluded in Section 4.

Governing Equations and Fine-scale Discretization

In this section, the governing equations for both rock matrix and fractures are described and the discretization of the coupled system of equations is explained.

Mass Balance

Mass balance equation for non-isothermal single-phase fluid flow reads

$$\frac{\partial}{\partial t}\left(\phi^{m}\rho_{f}\right)-\nabla\cdot\left(\rho_{f}\frac{1}{\mu_{f}}\mathbf{K}^{m}\cdot\nabla p^{m}\right)=\rho_{f}q^{mw}+\sum_{i=1}^{n_{\text{frac}}}\rho_{f}^{*}\,Q^{mf_i}, \tag{1}$$

for the rock matrix (m) and

$$\frac{\partial}{\partial t}\left(\phi^{f_i}\rho_{f}\right)-\nabla\cdot\left(\rho_{f}\frac{1}{\mu_{f}}\mathbf{K}^{f_i}\cdot\nabla p^{f_i}\right)=\rho_{f}q^{f_iw}+\rho_{f}^{*}\,Q^{f_im}+\sum_{j=1}^{n_{\text{frac}}}\left(\rho_{f}^{*}Q^{f_if_j}\right)_{j\neq i}, \tag{2}$$

for the lower dimensional fracture (f_i). Here, ϕ and $\mathbf{K}$ are the porosity and permeability of the medium. Note that $\mathbf{K}$ is a tensor. Superscripts m, f_i and w denote matrix, fracture i and well, respectively. Subscripts f corresponds to fluid, and ρ and μ are the density and viscosity of the fluid respectively. Moreover, q^{mw} and q^{f_iw} are the source terms (i.e., wells). Finally, Q^{mf_i} and Q^{f_im} are the flux exchange between fracture f_i and its overlapping matrix element m. Note that $Q^{f_if_j}$ is the flux from j-th fracture to the i-th fracture. The mentioned flux exchange terms are non-zero only where matrix-fracture overlap or fracture-fracture intersection exists. Due to mass conservation, $\iiint_{V} Q^{mf_i}dV=-\iint_{A_{f_i}} Q^{f_im}dA$, and $\frac{1}{}\iint_{A_{f_i}} Q^{f_if_j}dA=-\iint_{A_{f_j}} Q^{f_jf_i}dA$ hold.

The source terms q^{mw} and q^{f_iw} are modeled via Peaceman formulation (Peaceman, 1978) as

$$q^{mw}=\frac{PI\cdot\lambda^{*}\cdot(p^{w}-p^{m})}{V},\; q^{f_iw}=\frac{PI\cdot\lambda^{*}\cdot(p^{w}-p^{f_i})}{A}, \tag{3}$$

where, PI is the well productivity index. λ^* is the effective mobility between the source term and the medium. Moreover, the flux exchanges Q^{mf_i}, Q^{f_im} and $Q^{f_if_j}$ are defined as

$$Q^{mf_i}=CI^{mf_i}\cdot\lambda^{*}\cdot(p^{f_i}-p^{m}) \tag{4}$$

$$Q^{mf_i} = CI^{f_i m} \cdot \lambda^* \cdot (p^m - p^{f_i}) \tag{5}$$

$$Q^{f_i f_j} = CI^{f_i f_j} \cdot \lambda^* \cdot (p^{f_j} - p^{f_i}), \tag{6}$$

where CI is the connectivity index between the corresponding neighbouring elements (Hajibeygi et al., 2011b). As an example, the connectivity index between i-th matrix element and j-th fracture element is calculated as $CI_{ij} = \frac{A_{ij}}{\langle d \rangle_{ij}}$, where A_{ij} is the area fraction of fracture cell j overlapping with matrix cell i and $\langle d \rangle_{ij}$ is the average distance between these cells (Tene et al., 2016; HosseiniMehr et al., 2018).

Energy Balance for Fluid

Energy balance for fluid reads

$$\frac{\partial}{\partial t}\left(\phi^m \rho_f U_f^m\right) - \nabla \cdot \left(\rho_f H_f^m \frac{1}{\mu_f} \mathbf{K}^m \cdot \nabla p^m\right) - \nabla \cdot \left(\phi^m \mathbf{D}_f^m \cdot \nabla T_f^m\right) = Ah(T_r^m - T_f^m) + \rho_f H_f^m q^{mw} + \sum_{i=1}^{n_{\text{frac}}} \rho_f^* H_f^* Q^{mf_i}, \tag{7}$$

in the rock matrix (m) and

$$\frac{\partial}{\partial t}\left(\phi^{f_i} \rho_f U_f^{f_i}\right) - \nabla \cdot \left(\rho_f H_f^{f_i} \frac{1}{\mu_f} \mathbf{K}^{f_i} \cdot \nabla p^{f_i}\right) - \nabla \cdot \left(\phi^{f_i} \mathbf{D}_f^{f_i} \cdot \nabla T_f^{f_i}\right) = \rho_f H_f^{f_i} q^{f_i w} + \rho_f^* H_f^* Q^{f_i m} + \sum_{j=1}^{n_{\text{frac}}} \left(\rho_f^* H_f^* Q^{f_i f_j}\right)_{j \neq i} + Q_{T_f T_r}^{f_i m}, \tag{8}$$

in the lower dimensional fracture (f_i). Here, T_f and T_r are the fluid and solid rock temperature values, respectively. In addition, U_f and H_f are the specific internal energy and specific enthalpy in fluid, respectively, which can be expressed as non-linear functions of pressure temperature (Coats, 1977). D_f is the fluid thermal conductivity. The subscripts f and r indicate fluid and solid rock. A is the surface area involved in the heat exchange between fluid and solid phase in the rock, and h is the conduction-convection heat exchange coefficient between them. Note that the fracture porosity is assumed to be 1. Therefore the term $Ah(T_r^{f_i} - T_f^{f_i})$ is omitted from the fluid energy balance equation for fractures. Moreover, if the thermal equilibrium between rock and fluid is assumed, this term becomes zero. The conductive heat exchange at the porous surface of the fracture is denoted by $Q_{T_f T_r}^{f_i m}$, which is calculated as

$$Q_{T_f T_r}^{f_i m} = CI^{f_i m} \cdot \mathbf{D} \cdot (T_r^m - T_f^f). \tag{9}$$

Here, $\mathbf{D} = (1 - \phi^m)\mathbf{D}_r^m + \phi^{f_i}\mathbf{D}_f^{f_i}$ is the thermal conductivity of the saturated rock. Here, $\mathbf{D}_r$ is the rock thermal conductivity. Note that the fluid conductivity is assumed to be negligible compared with that of the solid rock.

Energy Balance for Solid Rock

Energy balance for solid rock reads

$$\frac{\partial}{\partial t}\left((1 - \phi)^m \rho_r U_r^m\right) - \nabla \cdot \left((1 - \phi^m)\mathbf{D}_r^m \cdot \nabla T_r^m\right) = Ah(T_f^m - T_r^m) + \sum_{i=1}^{n_{\text{frac}}} Q_{T_f T_r}^{mf_i}. \tag{10}$$

Here, ρ_r and U_r are density and specific internal energy of the solid rock, respectively. The heat exchange term $Q_{T_f T_r}^{mf_i}$ is obtained as

$$Q_{T_f T_r}^{mf_i} = CI^{mf_i} \cdot \mathbf{D} \cdot (T_f^f - T_r^m), \tag{11}$$

to balance the conductive heat exchange of Eq. (9). Note that there is no solid phase in the fractures, as such, the energy balance equation for rock only exists for the reservoir matrix.

Fine-scale Discrete System

The coupled discrete system of equations for Eqs. (1), (2), (7), (8) and (10) with three main unknowns of p, T_f and T_r is obtained using a two-point-flux-approximation (TPFA) finite-volume scheme in space and a backward (implicit) Euler scheme in time (Aziz and Settari, 2002). Independent structured grids are generated for porous medium and fractures. Non-linear FIM systems are solved using Newton-Raphson iterative scheme (Aziz and Settari, 2002).

Residual of mass balance equation for matrix (r^m_{MB}) and fractures ($r^{f_i}_{MB}$), residual of fluid energy balance equation for matrix (r^m_{EBF}) and fractures ($r^{f_i}_{EBF}$), and residual of energy balance equation for solid rock (r^m_{EBR}) form the full residual vector at time-step n as

$$r^n = [(r^m_{MB})^n, (r^{f_1}_{MB})^n, (r^{f_2}_{MB})^n, ..., (r^{f_{n_{\text{frac}}}}_{MB})^n, (r^m_{EBF})^n, (r^{f_i}_{EBF})^n, (r^m_{EBR})^n]^T. \tag{12}$$

The vector of pressure unknowns at time-step n is denoted as $[(p^m)^n, (p^{f_1})^n, (p^{f_2})^n, ..., (p^{f_{n_{\text{frac}}}})^n]^T$. Similarly, the temperature values are defined as $[(T^m_f)^n, (T^{f_1}_f)^n, (T^{f_2}_f)^n, ..., (T^{f_{n_{\text{frac}}}}_f)^n]^T$ for fluid and $[(T^m_m)^n]^T$ for the solid rock. The nonlinear equation $r^{n+1} = 0$ is solved iteratively as

$$r^{\nu+1} = r^\nu + \frac{\partial r}{\partial p}\bigg|^\nu \delta p^{\nu+1} + \frac{\partial r}{\partial T_f}\bigg|^\nu \delta T_f^{\nu+1} + \frac{\partial r}{\partial T_r}\bigg|^\nu \delta T_r^{\nu+1} = 0, \tag{13}$$

where the index ν denotes the iteration stage. At every Newton iteration, the set of all linearized equations can be written as a linear system $\mathbf{J}^\nu \delta x^{\nu+1} = -r^\nu$, where, $\mathbf{J}^\nu$ is the Jacobian matrix with $\delta x^{\nu+1} = [\delta p, \delta T_f, \delta T_r]^T$. As a whole, the mentioned linear system of equations is presented as the following

$$\underbrace{\begin{pmatrix} \begin{pmatrix} J^{mm}_{MB_p} & J^{mf}_{MB_p} \\ J^{fm}_{MB_p} & J^{ff}_{MB_p} \end{pmatrix} & \begin{pmatrix} J^{mm}_{MB_{T_f}} & J^{mf}_{MB_{T_f}} \\ J^{fm}_{MB_{T_f}} & J^{ff}_{MB_{T_f}} \end{pmatrix} & \begin{pmatrix} J^{mm}_{MB_{T_r}} \\ J^{fm}_{MB_{T_r}} \end{pmatrix} \\ \begin{pmatrix} J^{mm}_{EBF_p} & J^{mf}_{EBF_p} \\ J^{fm}_{EBF_p} & J^{ff}_{EBF_p} \end{pmatrix} & \begin{pmatrix} J^{mm}_{EBF_{T_f}} & J^{mf}_{EBF_{T_f}} \\ J^{fm}_{EBF_{T_f}} & J^{ff}_{EBF_{T_f}} \end{pmatrix} & \begin{pmatrix} J^{mm}_{EBF_{T_r}} \\ J^{fm}_{EBF_{T_r}} \end{pmatrix} \\ \begin{pmatrix} J^{mm}_{EBR_p} & J^{mf}_{EBR_p} \end{pmatrix} & \begin{pmatrix} J^{mm}_{EBR_{T_f}} & J^{mf}_{EBR_{T_f}} \end{pmatrix} & \begin{pmatrix} J^{mm}_{EBR_{T_r}} \end{pmatrix} \end{pmatrix}^\nu}_{\mathbf{J}^\nu_0} \underbrace{\begin{pmatrix} \delta p^m \\ \delta p^f \\ \delta T^m_f \\ \delta T^f_f \\ \delta T^f_r \end{pmatrix}^{\nu+1}}_{\delta x^{\nu+1}_0} = - \underbrace{\begin{pmatrix} r^m_{MB} \\ r^f_{MB} \\ r^m_{EBF} \\ r^f_{EBF} \\ r^m_{EBR} \end{pmatrix}^\nu}_{r^\nu_0} \tag{14}$$

Here, $\mathbf{J}^\nu_0$, $\delta x^{\nu+1}_0$ and r^ν_0 are the Jacobian (derivatives) matrix, the vector of updates and the residual vector, respectively. Also, each block J_{e_α} contains the derivatives of equation e with respect to the unknown α, i.e. $J_{e_\alpha} = \partial r_e / \partial \alpha$. Subscripts MB, EBF and EBR refer to equations of mass balance, energy balance in fluid and energy balance in the rock, respectively. Note that $J_{MB_{T_r}} = 0$ holds, as in the mass balance equation, the fluid properties do not depend on the rock temperature T_r.

In this work, to reach the non-linear convergence the following conditions have to be satisfied:

$$\frac{||r_{(MB)}||_2}{||r^0_{(MB)}||_2} < \varepsilon_{(MB)} \ \wedge \ \frac{||r_{(EBF)}||_2}{||r^0_{(EBF)}||_2} < \varepsilon_{(EBF)} \ \wedge \ \frac{||r_{(EBR)}||_2}{||r^0_{(EBR)}||_2} < \varepsilon_{(EBR)} \ \wedge \ \frac{||\delta p||_2}{||p||_2} < \varepsilon_{(p)} \ \wedge \ \frac{||\delta T_f||_2}{||T_f||_2} < \varepsilon_{(T_f)} \ \wedge \ \frac{||\delta T_r||_2}{||T_r||_2} < \varepsilon_{(T_r)} \tag{15}$$

Here, each of the aforementioned thresholds (ε_x) are user-defined tolerances given as input to the simulator.

Note that one can combine the energy balance for fluid and rock, under local thermal equilibrium assumption, so that only one temperature value exists as the main unknown of the energy equation. This

can be achieved at linear stage by clustering the corresponding rows and columns associated (resembles a CPR-based approach (Wallis et al., 1985; Cao et al., 2005)).

As mentioned before, the solution of the linear-system (14) is the most computationally expensive step for field-scale simulations. To resolve this challenge, field-scale relevant simulation approaches aim to develop a scalable solution strategy for this coupled nonlinear system. Therefore, the FG-ADM method is presented in the following section.

ADM Method for Fractured Geothermal system (FG-ADM)

The linear system of equations (14) is described and solved on a fully-resolved fine-scale discrete grid. FG-ADM method provides an alternative solution to the fine-scale system by constructing an algebraically reduced system on a dynamic multilevel grid resolution, which is defined at the beginning of every time-step. The resolution of this ADM system is obtained based on a front-tracking (or gradient of solution) error-estimation strategy. Let us assume that N_m grid cells are imposed on the matrix and $N_{f_{total}} = \sum_{i=1}^{n_{\text{frac}}} N_{f_i}$ fine-scale grid cells are imposed on the fractures. The fine-scale domain is obtained at level $l = 0$. Let N_m^l be the number of the grid cells in the matrix and $N_{f_i}^l$ the number of the grid cells in fracture i, both at level l. The coarsening ratio, γ^l (at coarsening level l) can therefore be defined as

$$\gamma^l = \left(\gamma_m^l, \gamma_{f_1}^l, \cdots, \gamma_{n_{\text{frac}}}^l\right) = \left(\frac{N_m^l}{N_m^{l-1}}, \frac{N_{f_1}^l}{N_{f_1}^{l-1}}, \cdots, \frac{N_{f_{n_{\text{frac}}}}^l}{N_{f_{n_{\text{frac}}}}^{l-1}}\right). \tag{16}$$

Note that the coarsening ratios for matrix and fracture f_i are, respectively, $\gamma_m^l = (\frac{N_{m_x}^l}{N_{m_x}^{l-1}} \times \frac{N_{m_y}^l}{N_{m_y}^{l-1}} \times \frac{N_{m_z}^l}{N_{m_z}^{l-1}})$ and $\gamma_{f_i}^l = (\frac{N_{f_{i\xi_i}}^l}{N_{f_{i\xi_i}}^{l-1}} \times \frac{N_{f_{i\eta_i}}^l}{N_{f_{i\eta_i}}^{l-1}})$. The coarsening level and the ratios for matrix and fractures are defined independently.

FG-ADM Operators

The ADM map between the fine-scale system to the dynamic multilevel grid resolution is obtained by applying sequences of restriction (**R**) and prolongation (**P**) operators across multiple levels, which are assembled from the local basis functions constructed only at the beginning of the simulation. In other words, at every iteration, the FG-ADM system is assembled as

$$\underbrace{\hat{\mathbf{R}}_l^{l-1} \dots \hat{\mathbf{R}}_1^0 \mathbf{J_0} \hat{\mathbf{P}}_0^1 \dots \hat{\mathbf{P}}_{l-1}^l}_{\mathbf{J}_{(FG-ADM)}} \delta\hat{x}_l = -\underbrace{\hat{\mathbf{R}}_l^{l-1} \dots \hat{\mathbf{R}}_1^0 r_0}_{r_l}. \tag{17}$$

Here, $\hat{\mathbf{R}}_l^{l-1}$ is the restriction operator mapping part of the vector of solutions which are at resolution $l-1$ ($\delta\hat{x}_{l-1}$) to resolution l($\delta\hat{x}_l$), and $\hat{\mathbf{P}}_{l-1}^l$ is the prolongation operator mapping part of the solution vector from level l to level l - 1. The solution of FG-ADM linear system (17) is then mapped to fine-scale as an approximated resolution $\delta x_0'$ (the reference fine-scale solution is represented as δx_0) using sequences of prolongation operators. More precisely:

$$\delta x_0 \approx \delta x_0' = \hat{\mathbf{P}}_0^1 \dots \hat{\mathbf{P}}_{l-1}^l \delta x_l. \tag{18}$$

In the FG-ADM method, the static multilevel multiscale prolongation operator $\mathbf{P}_{l-1}^l$ is constructed on the entire domain, which maps the solution from level l to l - 1. However, at each time step, the dynamic grid is obtained in such a way that only a specific part of the domain is mapped between the mentioned resolutions. This map is presented as $\hat{\mathbf{P}}_{l-1}^l$ in Eq. (17) and (18), which is referred to as ADM prolongation operator.

This static multilevel multiscale prolongation operator is a matrix including the blocks of prolongation operators for all unknowns (i.e., p, T_f, T_r), and reads:

$$\mathbf{P}_{l-1}^{l}=\begin{pmatrix}[(\mathbf{P}_p)_{l-1}^{l}]^{mm} & [(\mathbf{P}_p)_{l-1}^{l}]^{mf} & 0 & 0 & 0\\ [(\mathbf{P}_p)_{l-1}^{l}]^{fm} & [(\mathbf{P}_p)_{l-1}^{l}]^{ff} & 0 & 0 & 0\\ 0 & 0 & [(\mathbf{P}_{T_f})_{l-1}^{l}]^{mm} & 0 & 0\\ 0 & 0 & 0 & [(\mathbf{P}_{T_f})_{l-1}^{l}]^{ff} & 0\\ 0 & 0 & 0 & 0 & [(\mathbf{P}_{T_r})_{l-1}^{l}]^{mm}\end{pmatrix}_{N_{l-1}\times N_l}. \tag{19}$$

Additionally, the static multilevel multiscale restriction operator reads:

$$\mathbf{R}_{l}^{l-1}=\begin{pmatrix}[\mathbf{R}_{l}^{l-1}]^{m} & 0 & 0 & 0 & 0\\ 0 & [\mathbf{R}_{l}^{l-1}]^{f} & 0 & 0 & 0\\ 0 & 0 & [\mathbf{R}_{l}^{l-1}]^{m} & 0 & 0\\ 0 & 0 & 0 & [\mathbf{R}_{l}^{l-1}]^{f} & 0\\ 0 & 0 & 0 & 0 & [\mathbf{R}_{l}^{l-1}]^{m}\end{pmatrix}_{N_l\times N_{l-1}}, \tag{20}$$

which is a finite-volume restriction operator to assure mass conservation, i.e.,

$$\mathbf{R}_{l}^{l-1}(s,t)=\begin{cases}1 & \text{if cell } s \text{ is inside coarser cell } t,\\ 0 & \text{otherwise.}\end{cases} \tag{21}$$

Note that different interpolators are used for each variable (Cusini et al., 2018a; HosseiniMehr et al., 2018). The pressure prolongation operator $(\mathbf{P}_p)_{l-1}^{l}$ uses fully-coupled multilevel multiscale basis functions, whereas the prolongation operator of fluid temperature $(\mathbf{P}_{T_f})_{l-1}^{l}$ uses constant interpolators, i.e., $(\mathbf{P}_{T_f})_{l-1}^{l}=(\mathbf{R}_{l}^{l-1})^{T}$, where the superscript T refers to the transpose operator. The prolongation operator of rock temperature $(\mathbf{P}_{T_r})_{l-1}^{l}$ is also assembled by using multilevel multiscale basis functions.

Grid Selection Criterion

FG-ADM uses a user-defined grid selection criterion for the dynamic grid resolution map. At each time step n, the grid resolution is selected explicitly (based on the solution at time-step n - 1) by employing a temperature based criterion. Assume Ω_l^I and Ω_l^J as the set of two neighboring coarse cells I and J at resolution level l, which contain the index of all finer resolution cells they include. Also, i and j are fine cell indices, belonging to the sets Ω_l^I and Ω_l^J, respectively. The quantity $\Delta\bar{T}_{IJ}$ can defined as

$$\Delta\bar{T}_{IJ}=max(|T_i-T_j|)\quad \forall i\in\Omega_l^I \text{ and } \forall j\in\Omega_l^J, \tag{22}$$

and a grid-block I at grid resolution level l is refined to resolution (l - 1) if

$$\Delta\bar{T}_{IN}>\text{tol}, \tag{23}$$

where, N indicates all grid-blocks at resolution l neighbouring cell I. For the numerical examples of this article, the variable used for the coarsening criterion is the fluid temperature. Additionally, refinement is imposed around wells to ensure that the effect of source terms is captured accurately.

Numerical Results

Numerical results of two fractured test cases (one homogeneous and one heterogeneous) are presented in this section for which the performance of the proposed FG-ADM method is investigated. For error analyses, the fine-scale solutions are considered as accurate reference ones.

All test cases share a two-dimensional (2D) 100m × 100m fractured domain. An identical fracture network consisting of 35 fracture lines is considered for both test cases. A cold water injector well is present in the bottom left corner of the reservoir whereas a production well is placed at the top right corner. Both injection and production wells are pressure-constrained with bottom hole pressures of 30MPa and 10MPa, for injection and production, respectively. Temperature of the injected water is at 300K, whereas the reservoir is at initial temperature of 400K. No-flow boundary condition holds for all boundaries. All simulations are run till 500 days of simulation time is reached and the results are reported every 20 days (25 reports). The fluid and rock properties used here are presented in Table 1. The Appendix section includes all the correlations used to compute the remaining fluid properties. Please note that here, we assume the fluid thermal conductivity is negligible.

Table 1—Fluid and rock properties.

Property	value
Rock thermal conductivity (D_r)	4 [W/m.K]
Fluid thermal conductivity (D_f)	negligible
Rock density ($\boldsymbol{\rho}_r$)	2750 [kg/m^3]
Rock specific heat (C_{pr})	790 [J/kg.K]
Porosity (ϕ)	0.2
Fractures permeability	10^{-8}m^2
Fractures aperture	10^{-3}m
Grain diameter	0.001 m
Fluid specific heat (C_{pf})	4200 [J/kg.K]

Fine-scale simulation is run on both test cases with local thermal equilibrium assumption, where only one average temperature is used for both rock and fluid. As mentioned, the results of the FG-ADM method is compared against those obtained by the fine-scale simulator. The performance of FG-ADM is represented in fraction of number of active grid cells compared to the total number of fine-scale grid cells. The FG-ADM error at time step t is calculated as

$$\varepsilon_x(t) = \frac{\|x_{FS}(t) - x_{ADM}(t)\|_2}{\|x_{FS}(t)\|_2}, \tag{24}$$

where, x represents a generic variable (i.e., pressure p or temperature T) and the subscript FS refers to fine-scale.

Test Case 1: 2D fractured reservoir with homogeneous permeability field

A homogeneous rock with isotropic permeability value of $K_m = 10^{-14}$ m^2 is considered. A 135 × 135 = 18225 Cartesian grid is imposed on the matrix and the fractures are discretised into 1665 grid cells in total. 3 coarsening levels for matrix and 2 coarsening levels for fractures are set, with coarsening ratio of 3 in each direction for both the matrix and the fractures. The differences of fluid temperatures between neighbouring cells is used as the coarsening criterion with four different threshold values of $\Delta T_f = \{5,10,20,50\}$.

Figure 1 shows the results of the fine-scale simulation using thermal equilibrium assumption.

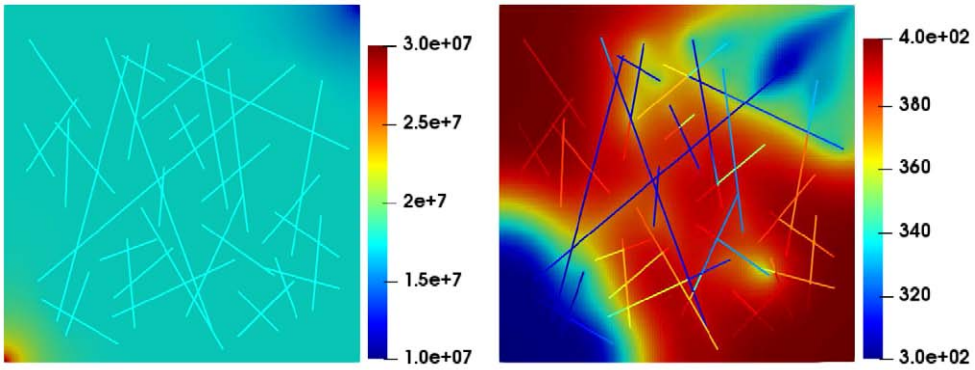

(a) Pressure - Fine Scale (b) Average Temperature - Fine Scale

Figure 1—Test case 1: Pressure and temperature plots for fine-scale solutions.

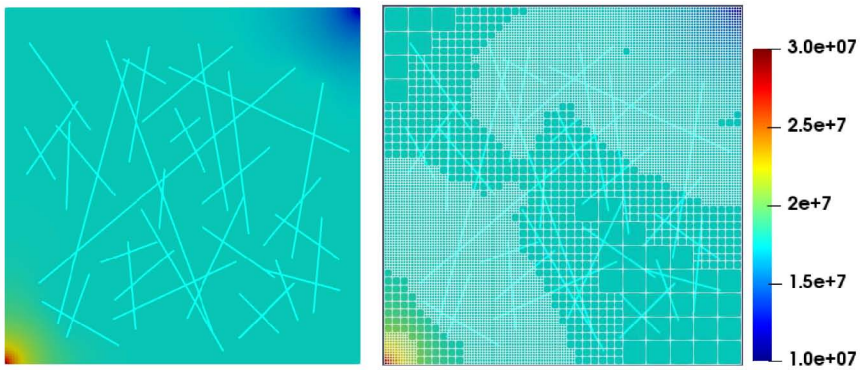

(a) Fine-scale (b) ADM $\delta T = 5$ error$= 1.50 \times 10^{-3}$

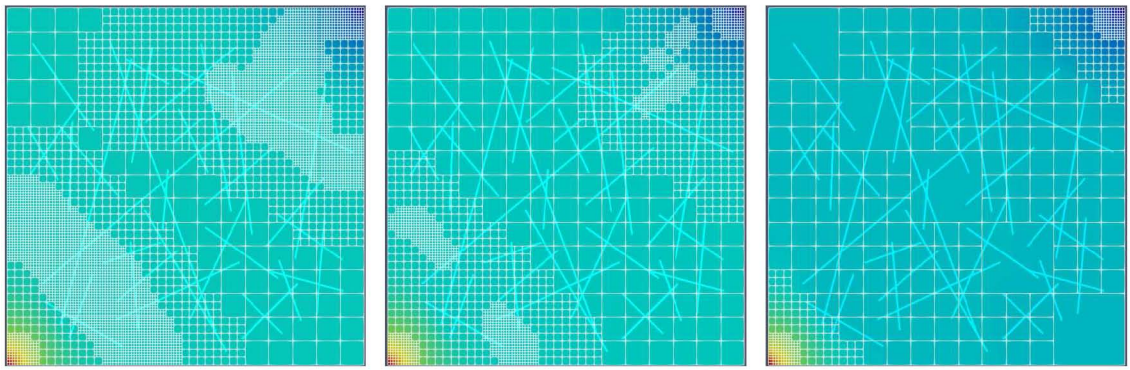

(c) ADM $\delta T = 10$ error$= 3.80 \times 10^{-3}$ (d) ADM $\delta T = 20$ error$= 7.70 \times 10^{-3}$ (e) ADM $\delta T = 50$ error$= 1.95 \times 10^{-2}$

Figure 2—Test case 1: fine-scale and ADM pressure plots with different threshold values δT.

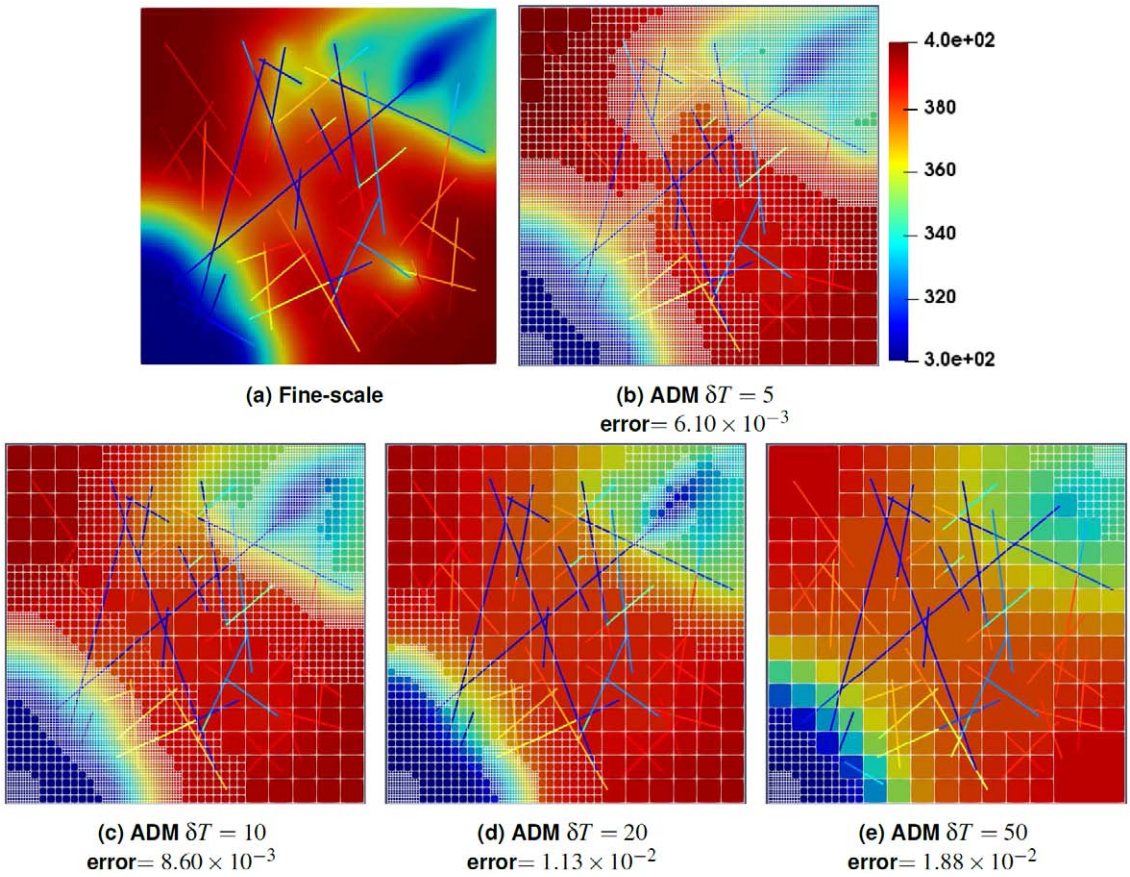

Figure 3—Test case 1: fine-scale and ADM temperature plots with different threshold values δ*T*.

Figures 2 and 3 show, respectively, the pressure and temperature results of fine-scale and FG-ADM simulations at final time-step ($t = 500$ days). Figure 4 shows the average pressure and temperature errors and the amount of active gird cells throughout the entire simulation time for all four chosen ADM grid selection criteria. Note that there is always 3.2% of active grid cells in the beginning of the simulation which is mainly due to the near-well grid refinement (the grid cells around wells are always kept at the fine-scale resolution).

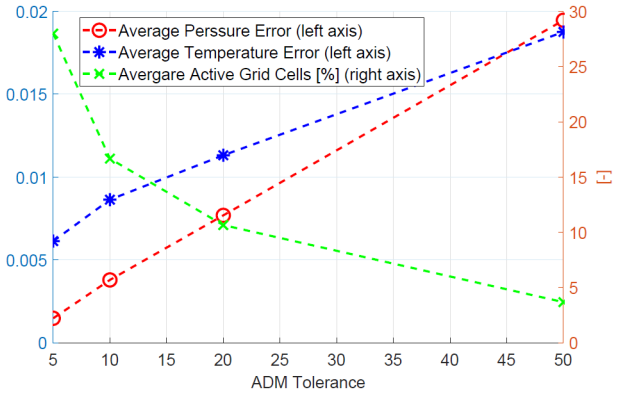

Figure 4—Test case 1: Average Errors and Active Grid Cells.

Test Case 2: heterogeneous permeability field

This test case consists of a heterogeneous matrix with permeability ranging from $min(K_m) = 5.9 \times 10^{-18}$m^2 to $max(K_m) = 4.2 \times 10^{-7}$m^2. A $81 \times 81 = 6561$ Cartesian grid is imposed on the matrix and the fractures are discretized into 1188 grid cells in total. Same as the previous test case, 3 coarsening levels for matrix

and 2 coarsening levels for fractures is considered, and coarsening ratio is 3 for the entire domain. Identical coarsening criterion as in the previous test case is employed for the ADM grid selection (ΔT_f= {5,10,20,50}).

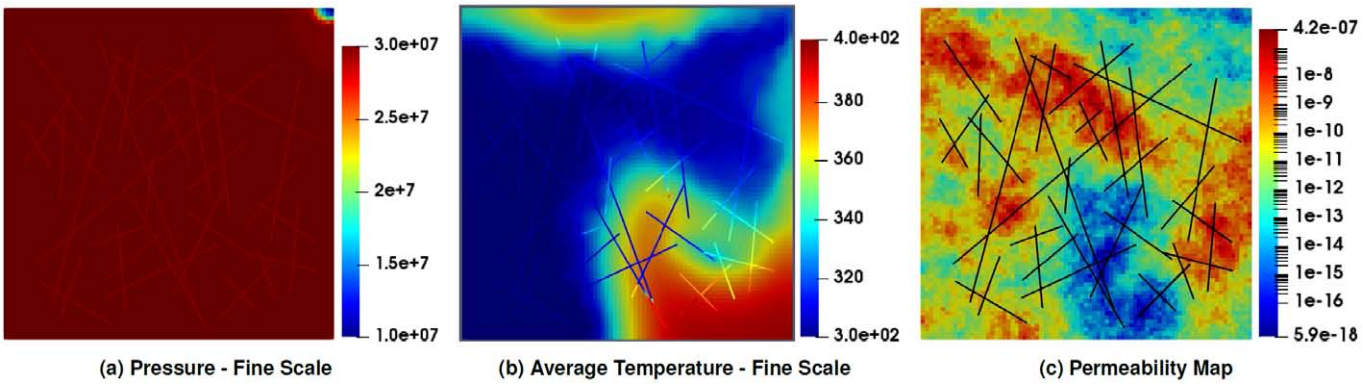

Figure 5—Test case 2: Pressure and temperature plots for fine-scale solutions.

The results of fine-scale simulation for heterogeneous test case are presented in figure 5.

For test case 2, pressure and temperature results of fine-scale together with four FG-ADM simulations are shown in figures 6 and 7. Similar to test case 1, all the simulations of this test case were run till t = 500days and the plots display the result for final time-step.

Figure 8 illustrates the average pressure and temperature errors as well as the average active grid cells employed by the ADM approach. For this test case, 7.3% of active grid cells are always considered in the beginning of simulation due to the fine-scale grid resolution near the injection and production wells.

Conclusion

An Algebraic Dynamic Multilevel method for fully-coupled simulation of single phase flow in fractured geothermal reservoirs (FG-ADM) was presented. Using the embedded discrete fracture model (EDFM), the fully implicit system in fine-scale discretization was mapped into a multilevel dynamic grid (independently defined for matrix and fractures) by employing a sequence of multilevel restriction and prolongation operators which are sets of local basis multilevel functions. These local basis functions were defined after selection of the coarse nodes on both matrix and fracture sub-domains on each coarsening level, with flexible matrix-fracture coupling. Using front-tracking technique, fine-scale grids were employed only where needed (i.e., around the wells and at the location of the temperature front) detected via the ADM grid selection criterion. However, different levels of coarse grids are employed wherever the fine-scale resolution is not needed. The use of multilevel multiscale basis functions guarantees the accuracy of the global unknowns where coarse grids are imposed. All basis functions were computed at the beginning of the simulation, and were reused during the entire simulation.

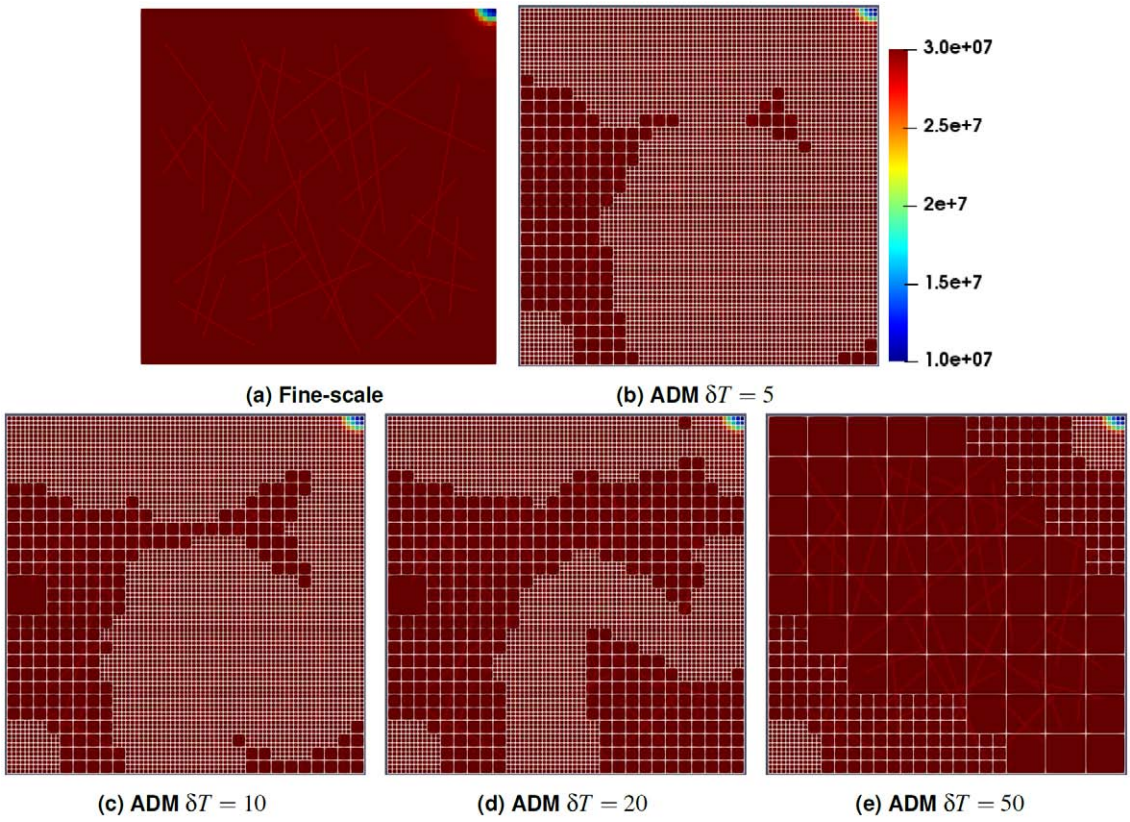

Figure 6—Test case 2: fine-scale and ADM pressure plots with different threshold values δT.

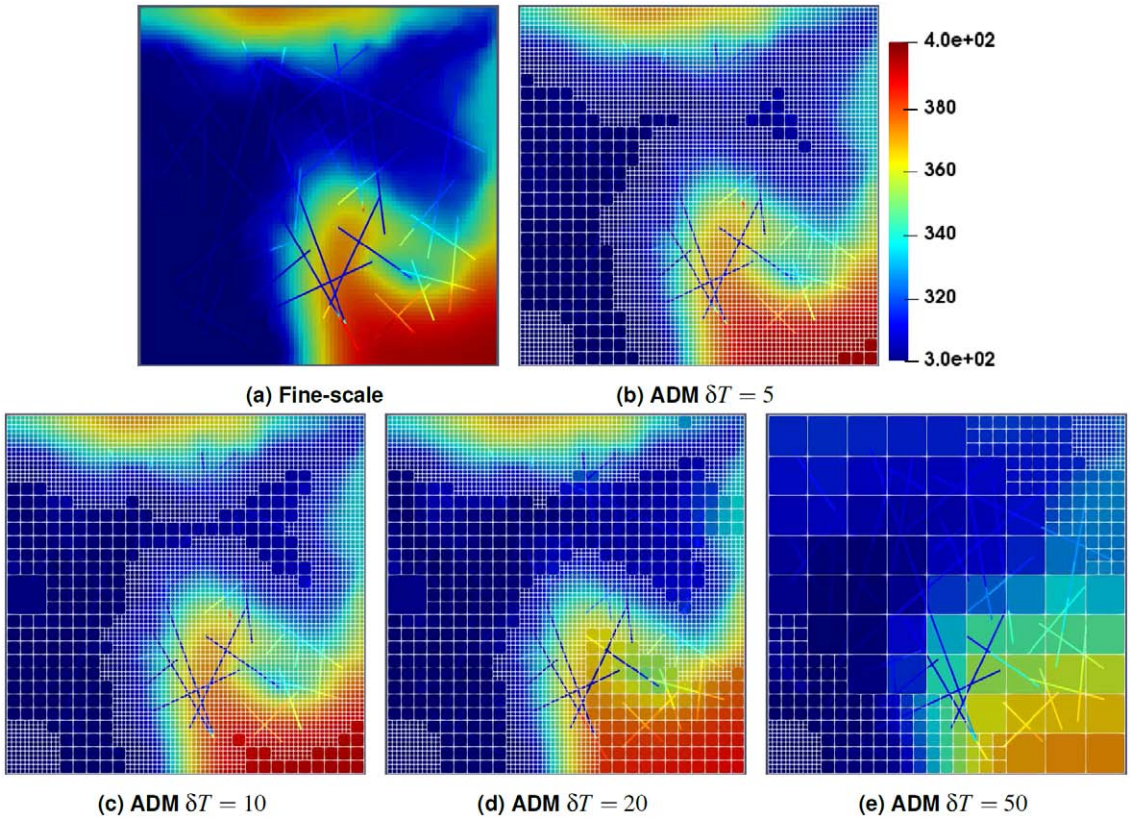

Figure 7—Test case 2: fine-scale and ADM temperature plots with different threshold values δT.

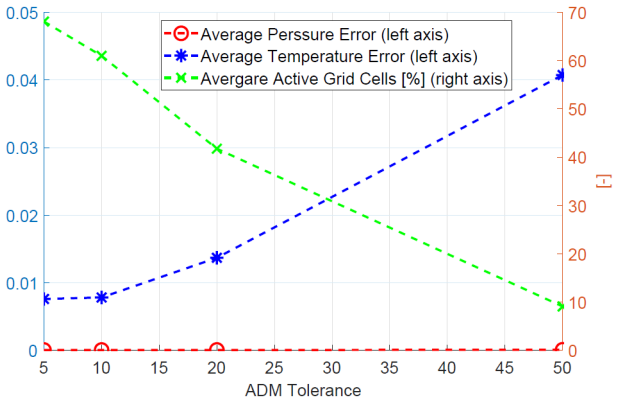

Figure 8—Test case 2: Average errors and active grid cells.

Numerical results for 2D homogeneous and heterogeneous fractured test cases were presented. FG-ADM results on both test cases were compared to those obtained from a fine-scale simulator. The sensitivity of FG-ADM to different grid coarsening criteria was also studied. The results, with different amount of dynamic active grid cells, show that FG-ADM is capable of providing accurate results by employing only a fraction of the fine-scale grid cells in the domain where needed. Due to the rarefaction of the temperature profile (highly diffused temperature fronts), more fine-scale grid cells are used at the front for heat transfer. In addition, the FG-ADM provides a robust algebraic framework which brings a scalable simulation method for thermal fluid flows. It is expected that by increasing the size of the domain, the average percentage of active grid cells reduces. Therefore, ADM casts a promising simulation approach for real-field geothermal reservoir simulations.

Acknowledgment

The authors thank the members of Delft Advanced Reservoir Simulation (DARSim) research group for all the fruitful discussions, feedback and all scientific comments during the successful development of FG-ADM method. The development of this work was implemented in DARSim2 Matlab Simulator. Interested researchers can obtain a free-licence open source copy of DARSim2 Simulator by contacting Dr. Hadi Hajibeygi.

References

Al-Shemmeri, T. (2012). Engineering Fluid Mechanics, **chapter 1**, page 18. Bookboon.

Aziz, K. and Settari, A. (2002). Petroleum Reservoir Simulation. *Blitzprint Ltd., Calgary, Alberta*.

Bell, J. and Shubin, G. (1983). An adaptive grid finite difference method for conservation laws. *J. Comput. Phys.*, **52**:569–591.

Berger, M. and Oliger, J. (1984). Adaptive mesh refinement for hyperbolic partial differential equations. *J. Comput. Phys.*, **53**:484–512.

Bertani, R. (2012). Geothermal power generation in the world 2005-2010 update report. *Geothermics*, **41**:1–29.

Burnell, J., Clearwater, E., A., C., Kissling, W., OSullivan, J., OSullivan, M., and Yeh, A. (2012). Future directions in geothermal modelling. In In Proceedings (electronic) 34rd New Zealand Geothermal Workshop, pages 19–21.

Burnell, J., OSullivan, M., OSullivan, J., Kissling, W., Croucher, A., Pogacnik, J., Pearson, S., Caldwell, G., Ellis, S., Zarrouk, S., and Climo, M. (2015). Geothermal supermodels: the next generation of integrated geophysical, chemical and flow simulation modelling tools. In In Proceedings World Geothermal Congress, pages 19–21.

Cao, H., Tchelepi, H. A., Wallis, J. R., and Yardumian, H. (2005). Constrained residual acceleration of conjugate residual methods. SPE paper 96809, SPE Annual Technical Conference and Exhibition, Dallas, Texas, USA.

Coats, K. H. (1977). Geothermal Reservoir Modelling. In SPE Annual Fall Technical Conference and Exhibition.

Cusini, M., Fryer, B., van Kruijsdijk, C., and Hajibeygi, H. (2018a). Algebraic dynamic multilevel method for compositional flow in heterogeneous porous media. *J. Comput. Phys.*, **354**:593–612.

Cusini, M., Gielisse, R., Groot, H., van Kruijsdijk, C., and Hajibeygi, H. (2018b). Incomplete mixing in porous media: Todd-longstaff upscaling approach versus a dynamic local grid refinement method. *Computational Geosciences*, 10.1007/s10596-018-9802-0.

Cusini, M., van Kruijsdijk, C., and Hajibeygi, H. (2016). Algebraic dynamic multilevel (adm) method for fully implicit simulations of multiphase flow in porous media. *Journal of Computational Physics*, **314**:60–79.

Dogru, A. H., Fung, L. S. K., Middya, U., Al-Shaalan, T., and Pita, J. A. (2009). A next-generation parallel reservoir simulator for giant reservoirs. 2009 SPE Reservoir Simulation Symposium, The Woodlands, Texas. 10.2118/119272-MS.

Edwards, M. (1996). A higher-order godunov scheme coupled with dynamical local grid refinement for flow in a porous medium. *Comput. Methods Appl. Mech Eng.*, **131**:287–308.

Faigle, B., Helmig, R., Aavatsmark, I., and Flemisch, B. (2014). Efficient multiphysics modelling with adaptive grid refinement using a mpfa method. *Computat. Geosci.*, **18**:625–636.

Fumagalli, A., Pasquale, L., Zonca, S., and Micheletti, S. (2016). An upscaling procedure for fractured reservoirs with embedded grids. *Water Resources Research*, **52**(8):6506–6525.

Fumagalli, A., Zonca, S., and Formaggia, L. (2017). Advances in computation of local problems for a flow-based upscaling in fractured reservoirs. *Mathematics and Computers in Simulation*, **137**:299–324.

Fung, L. S. K. and Dogru, A. H. (2007). Parallel unstructered solver methods for complex giant reservoir simulation. SPE paper 106237, SPE Reservoir Simulation Symposium, Houston, Texas, USA.

Garipov, T. T., Karimi-Fard, M., and Tchelepi, H. A. (2016). Discrete fracture model for coupled flow and geomechanics. *Computational Geosciences*, **20**(1):149–160.

Hajibeygi, H., Bonfigli, G., Hesse, M., and Jenny, P. (2008). Iterative multiscale finite-volume method. *J. Comput. Phys.*, **227**:8604–8621.

Hajibeygi, H., Karvounis, D., and Jenny, P. (2011a). A hierarchical fracture model for the iterative multiscale finite volume method. *J. Comput. Phys.*, **230**(24):8729–8743.

Hajibeygi, H., Karvounis, D., and Jenny, P. (2011b). A hierarchical fracture model for the iterative multiscale finite volume method. *Journal of Computational Physics*, **230**(24):8729–8743.

Hornung, R. and Trangenstein, J. (1997). Adaptive mesh refinement and multilevel iteration for flow in porous media. *J. Comput. Phys.*, **136**:522–545.

HosseiniMehr, M., Cusini, M., Vuik, C., and Hajibeygi, H. (2018). Algebraic dynamic multilevel method for embedded discrete fracture model (f-adm). *Journal of Computational Physics*, **373**:324–345.

Hou, T. Y. and Wu, X.-H. (1997). A multiscale finite element method for elliptic problems in composite materials and porous media. *J. Comput. Phys.*, **134**:169–189.

Jenny, P., Lee, S. H., and Tchelepi, H. A. (2003). Multi-scale finite-volume method for elliptic problems in subsurface flow simulation. *J. Comput. Phys.*, **187**:47–67.

Jiang, J. and Younis, R. M. (2016). Hybrid coupled discrete-fracture/matrix and multicontinuum models for unconventional-reservoir simulation. *SPE Journal*, **21**(03):1009–1027.

Klemetsdal, O., Moyner, O., and Lie, K.-A. (2018). Use of dynamically adapted basis functions to accelerate multiscale simulation of complex geomodels. ECMOR XVI - 16th European Conference on the Mathematics of Oil Recovery. http://dpi.org/10.3997/2214-4609.201802251.

Leal, A. M. M., Kulik, D. A., Smith, W. R., and Saar, M. O. (2017). An overview of computational methods for chemical equilibrium and kinetic calculations for geochemical and reactive transport modeling. *Pure and Applied Chemistry*, **89**(5):597–643.

Lee, S., Lough, M., and Jensen, C. (2001). Hierarchical modeling of flow in naturally fractured formations with multiple length scales. *Water Resource Research*, **37**(3):443–455.

Lee, S. H., Jensen, C. L., and Lough, M. F. (1999). An efficient finite difference model for flow in a reservoir with multiple length-scale fractures. *SPEATCE*.

Li, L. and Lee, S. H. (2008). Efficient field-scale simulation of black oil in naturally fractured reservoir through discrete fracture networks and homogenized media. *SPE Reservoir Evaluation and Engineering*, pages 750–758.

Lund, J. W., Freeston, D. H., and Boyd, T. L. (2011). Direct utilization of geothermal energy 2010 worldwide review. *Geothermics*, **40**(3):159–180.

McClure, M. W. and Horne, R. N. (2014). An investigation of stimulation mechanisms in enhanced geothermal systems. *International Journal of Rock Mechanics and Mining Sciences*, **72**:242–260.

Moinfar, A., Varavei, A., Sepehrnoori, K., and Johns, R. T. (2014). Development of an efficient embedded discrete fracture model for 3d compositional reservoir simulation in fractured reservoirs. *SPE J.*, **19**:289–303.

Moraes, R., Rodrigues, J., Hajibeygi, H., and Jansen, J. (2017). Multiscale gradient computation for flow in heterogeneous porous media. *J. Comp. Phys.*, **336**(6):644–663.

Morel, F. and Morgan, J. (1972). Numerical method for computing equilibriums in aqueous chemical systems. *Environmental Science & Technology*, **6**(1):58–67.

Nield, D. A. and Bejan, A. (2006). *Convection in Porous Media*. Springer.

Norbeck, J. H., McClure, M. W., Lo, J. W., and Horne, R. N. (2016). An embedded fracture modeling framework for simulation of hydraulic fracturing and shear stimulation. *Computational Geosciences*, **20**(1):1–18.

Peaceman, D. W. (1978). Interpretation of well-block pressures in numerical reservoir simulation. *SPE J.*, **18** (3):183–194.

Pluimers, S. (2015). Hierarchical fracture modeling. Msc thesis, Delft University of Technology, The Netherlands.

Praditia, T., Helmig, R., and Hajibeygi, H. (2018). Multiscale formulation for couple. *Computat. Geo., (in press)*:DOI: 10.1007/s10596-018-9754-4.

Rossi, E., Kant, M. A., Madonna, C., Saar, M. O., and von Rohr, P. R. (2018). The effects of high heating rate and high temperature on the rock strength: Feasibility study of a thermally assisted drilling method. *Rock Mechanics and Rock Engineering*.

Sammon, P. H. (2003). Dynamic grid refinement and amalgamation for compositional simulation. in: SPE Reservoir Simulation Symposium, 21-23 February, The Woodlands, Texas, USA, **2003**, SPE paper 79683,, pages 1–11.

Schmidt, G. and Jacobs, F. (1988). Adaptive local grid refinement and multi-grid in numerical reservoir simulation. *J. Comput. Phys.*, **77**:140–165.

Shah, S., Moyner, O., Tene, M., Lie, K.-A., and Hajibeygi, H. (2016). The multiscale restriction smoothed basis method for fractured porous media (f-msrsb). *Journal of Computational Physics*, **318**:36–57.

Singh, G., Leung, W., and Wheeler, M. (2018). Multiscale methods for model order reduction of non-linear multiphase flow problems. *Comput Geosci.* 10.1007/s10596-018-9798-5.

Tene, M., Al Kobaisi, M. S., and Hajibeygi, H. (2016). Algebraic multiscale method for flow in heterogeneous porous media with embedded discrete fractures (f-ams). *Journal of Computational Physics*, **321**:819–845.

Tene, M., Bosma, S. B., Kobaisi, M. S. A., and Hajibeygi, H. (2017). Projection-based embedded discrete fracture model (pedfm). *Advances in Water Resources*, **105**:205–216.

van Batenburg, D., Bosch, M., Boerrigter, P., de Zwart, A., and Vink, J. (2011). Application of dynamic gridding techniques to IOR/EOR processes. in: SPE Reservoir Simulation Symposium, 21-23 February, The Woodlands, Texas, USA, **2011**, SPE paper 141711, pages 1–16.

Wagner, W. and Kretzschmar, H. (2008). *International Steam Tables - Properties of Water and Steam based on the Industrial Formulation IAPWS-IF97*. Springer, second edition.

Wallis, J. R., Kendall, R. P., Little, T. E., and Nolen, J. S. (1985). Constrained residual acceleration of conjugate residual methods. SPE Reservoir Simulation Symposium, 10.2118/13536-MS.

Wang, Y., Hajibeygi, H., and Tchelepi, H. A. (2014). Algebraic multiscale linear solver for heterogeneous elliptic problems. *J. Comput. Phys.*, **259**:284–303.

Wong, Z. Y., Horne, R. N., and Tchelepi, H. A. (2018). Sequential implicit nonlinear solver for geothermal simulation. *Journal of Computational Physics*, **368**:236–253.

Younis, R., Tchelepi, H. A., Aziz, K., et al (2010). Adaptively localized continuation-newton method-nonlinear solvers that converge all the time. *SPE Journal*, **15**(02):526–544.

Zeng, Z. and Grigg, R. (2006). A Criterion for Non-Darcy Flow in Porous Media. In *Transport in Porous Media*, volume **63**, pages 57–69.

Appendix

correlations

The following correlations were employed to compute fluid and rock properties in the numerical experiments.

Fluid viscosity: Viscosity-temperature relationship reads (Al-Shemmeri, 2012)

$$\mu_f(T) = 2.414 \times 10^{-5} \times 10^{\frac{247.8}{T-140}}.$$

Fluid density: Fluid density is defined as function of pressure and temperature (Coats, 1977) as

$$\rho_f(P,T) = \rho_{fs}(T)\left[1 + c_w(T)(P - P_s)\right],$$

where $P_S = 1$ bar. $c_w(T)$ and $\rho_{fs}(T)$ are obtained from empirical correlations (Praditia et al., 2018; Wagner and Kretzschmar, 2008), i.e.,

$$c_w(T) = \left(0.0839T^2 + 652.73T - 203714\right) \times 10^{-12}$$

$$\rho_{fs}(T) = -0.0032T^2 + 1.7508T + 757.5.$$

Fluid Entalphy: Fluid enthalpy is defined as function of pressure and temperature (Coats, 1977) as

$$H_f(P,T) = u_{ws} + C_{pf}(T - T_s) + \frac{P}{\rho_f},$$

where $u_{ws} = 420000 \frac{\mathrm{J}}{\mathrm{kg}}$.

Heat exchange coefficient: Heat exchange coefficient h is given as (Nield and Bejan, 2006)

$$\frac{1}{h} = \frac{D_p}{N_u k_f} + \frac{D_p}{10\,D},$$

where D_p is the grain diameter and D is the rock heat conductive coefficient. In this work, the fluid conductivity (only used for this equation) is set as $k_f = 0.591$W/m.K. Note that N_u is the Nusselt number, which is defined as

$$N_u = \frac{0.225}{\phi} P_r^{0.33} R_e^{0.67},$$

where P_r (Nield and Bejan, 2006) and R_e (Zeng and Grigg, 2006) are the Prandtle and Reynolds numbers, respectively, i.e.,

$$P_r = \frac{C_{pf}\mu_f}{k_f}.$$

and

$$R_e = \frac{\rho_f V D_p}{\mu_f}.$$

Here V is the Darcy velocity.